Fractional Vegetation Cover Estimation Algorithm Based on Recurrent Neural Network for MODIS 250 m Reflectance Data

Duanyang Liu, Kun Jia, Mu Xia, Xiangqin Wei, Yunjun Yao, Xiaotong Zhang, and Guofeng Tao

***Abstract*—Fractional vegetation cover (FVC) is a critical land surface parameter, and several large-scale FVC products have been generated based on remote sensing data. Among these existing products, the global land surface satellite (GLASS) FVC product, derived from moderate resolution imaging spectroradiometer (MODIS) 500 m reflectance data (MOD09A1), has achieved complete spatial-temporal continuity and satisfying accuracy. To further improve the spatial resolution of GLASS FVC product, this study developed a novel FVC estimation algorithm for MODIS 250 m reflectance data based on a recurrent neural network with the long short-term memory unit (RNN-LSTM). The RNN-LSTM was established using sequence training samples derived from the MODIS 250 m reflectance and GLASS FVC products, which were conducted over three vegetation types in mid-West China. Additionally, two machine learning methods, including the back propagation neural network (BPNN) and multivariate adaptive regression splines (MARS), were used to compare with the proposed method. The evaluation results showed that RNN-LSTM derived FVC had reliable spatial-temporal continuity and good consistency with the GLASS FVC product. Furthermore, the smooth temporal profiles of the RNN-LSTM FVC estimation indicated that the proposed method was capable of capturing the temporal characteristics of vegetation growth and reducing the uncertainties from the atmosphere and radiation. Finally, an independent validation case in the Heihe area indicated that the RNN-LSTM algorithm achieved the best accuracy ($R^2 = 0.8081$, rmse $= 0.0951$) compared with the BPNN ($R^2 = 0.7320$, rmse $= 0.1127$) and MARS ($R^2 = 0.7361$, rmse $= 0.1117$). This study provides a new approach by showing the potential of the RNN-LSTM method for land surface parameter estimation and related research.**

***Index Terms*—Artificial intelligence, multivariate adaptive regression splines, neural networks, subpixel vegetation cover mapping.**

Manuscript received February 23, 2021; revised April 16, 2021; accepted April 21, 2021. Date of publication April 27, 2021; date of current version July 14, 2021. This work was supported in part by the National Key Research and Development Program of China under Grant 2016YFA0600103, Grant 2020YFE0200700 and Grant 2019YFE0127300. The work of Kun Jia was supported by the Tang Scholar of Beijing Normal University. *(Corresponding author: Kun Jia.)*

Duanyang Liu, Kun Jia, Mu Xia, Yunjun Yao, Xiaotong Zhang, and Guofeng Tao are with the State Key Laboratory of Remote Sensing Science, Faculty of Geographical Science and the Beijing Engineering Research Center for Global Land Remote Sensing Products, Faculty of Geographical Science, Beijing Normal University, Beijing 100875, China (e-mail: duanyangliu0505@mail.bnu.edu.cn; jiakun@bnu.edu.cn; xiamu@mail.bnu.edu.cn; boyyunjun@bnu.edu.cn; xtngzhang@bnu.edu.cn; 201921051079@mail.bnu.edu.cn).

Xiangqin Wei is with the Aerospace Information Research Institute, Chinese Academy of Sciences, Beijing 100101, China (e-mail: weixq@aircas.ac.cn).

Digital Object Identifier 10.1109/JSTARS.2021.3075624

I. Introduction

As THE essential component of the terrestrial ecosystem, vegetation plays a crucial role in energy exchange and biogeochemical and hydrological cycling processes [1]–[3]. Fractional vegetation cover (FVC), defined as the fraction of green vegetation as seen from nadir [4], is usually used to describe the growth state of land surface vegetation [5]. FVC plays an essential role in monitoring vegetation growth and driving the earth system models [6]–[9]. For example, FVC data contributed to the improvement of surface air temperature simulation in climate models [10], and reduced the prediction error of Budyko's hydrological model over medium spatial scales [11]. In addition, FVC was also utilized to explore the effect of climatic/human-induced factors on vegetation cover change in Beijing, China [12]. Therefore, large-scaled FVC estimation with high accuracy is essential to successfully model these land surface processes [9], [13], [14].

Due to its excellent ability to acquire earth observation data, remote sensing is a feasible and effective tool for long-term FVC estimation at either reginal or global scales [13], [15]. Currently, many large-scale and global FVC products have been developed using various methods and remote sensing data. For example, a linear inversion approach is adopted to generate the Polarization and Directionality of the Earth's Reflectances of National Centre for Space Studies (CNES/POLDER) FVC from Advanced Earth Observing Satellites (ADEOS) [14]. The linear relationship between FVC and difference vegetation index (DVI) is determined based on the simulation data generated by a kernel-driven model. However, because of the malfunction of ADEOS satellites, there are limited earth observation data for POLDER instrument, and the GNES/POLDER FVC product is only available for year 1996, 1997, and 2003 [14], [16]. The Satellite Application Facility on Land Surface Analysis (LSA SAF) FVC product of European Organization for the Exploitation of Meteorological Satellites (EUMETSAT) is generated through a probabilistic spectral mixture analysis method, and the product only covers Europe, Africa, and South America [17], [18]. Additionally, both the European Space Agency/Medium Resolution Imaging Spectrometer (ESA/MERIS) and Carbon Cycle and Change in Land Observational Products from an Ensemble of Satellites (CYCLOPES) FVC products are developed through neural network methods. Moreover, the training samples are obtained from the combination model of the leaf optical

This work is licensed under a Creative Commons Attribution 4.0 License. For more information, see https://creativecommons.org/licenses/by/4.0/

properties model PROSPECT and the scattering by arbitrarily inclined leaves (SAIL) model [19]–[21]. However, significant systemic underestimation is found in the CYCLOPES FVC product, and the MERIS FVC product is no longer generated after the completion of the project [17], [22]–[24]. According to the corrected CYCLOPES FVC product, three different versions of VGT bioGEOphysical FVC products (GEOV1, GEOV2, and GEOV3) are developed based on neural network methods [4], [25], [26]. As for these three FVC products, considerable amount of missing data are found in the GEOV1 and GEOV3 FVC products, especially during winter over high latitudes [27]. In addition, the GEOV2 FVC product also presents high uncertainties in low FVC values compared to the global field measurements [28]. Furthermore, the Global LAnd Surface Satellite (GLASS) FVC product is developed using the multivariate adaptive regression splines (MARS) method based on MODIS reflectance data, and the training sample data are generated from high spatial resolution data (Landsat TM/ETM+) with the pixel unmixing method [1], [29]. Validation and inter-comparison results indicate that the GLASS FVC product achieves stable spatiotemporal continuity and satisfactory accuracy [28]. However, an inevitable limitation of the GLASS FVC product is the spatial resolution, which is 500 m. Given that there are 250 m MODIS reflectance data, corresponding FVC products with the same spatial resolution are still lacking. Thus, it is significant to develop a reliable FVC estimation algorithm for MODIS 250 m reflectance data, which will effectively improve the spatial resolution and performance of the GLASS FVC product and promote further FVC applications to higher spatial resolution research.

At present, many FVC estimation algorithms have been proposed and used to generate FVC products based on remote sensing data over a large scale. Generally, these methods can be summarized in three main categories: empirical methods, pixel unmixing models, and machine learning methods. Usually, the empirical method estimates FVC values by calculating the regression relationship between FVC and reflectance of specific bands or vegetation indices, which presents satisfactory performance at small region for specific vegetation types [30]. However, the established empirical models have great uncertainties when they are applied at a large region, because the relationship is changed with various vegetation types and land conditions [31]. For pixel unmixing models, a basic assumption is that each pixel is composed of several components, referred to as endmembers, and the proportion of green vegetation components is considered as the corresponding FVC value [32]. With clear physical assumptions, pixel unmixing models are easy to understand and widely used for FVC estimation [31], [33]. However, due to the complex land surface conditions and complex spectral characteristics of various land objects over large region, it is difficult to determine the representative endmembers [34]. As for machine learning methods, FVC estimation models are built based on high-quality training samples. With stable computational efficiency and reliability for nonlinear fitting problems, machine learning methods, like artificial neural networks, MARS, and support vector regression, have been widely used in FVC product generation and land surface parameters retrieval, especially over large scales [4], [35]–[38].

Although the existing methods mentioned above have achieved a certain degree of accuracy in FVC estimation, a significant limitation of these methods is that they only employ the instantaneous reflectance or vegetation indices as input data during the FVC estimation process [39], [40]. Therefore, these methods insufficiently utilize the temporal characteristics and ignore the correlation in the vegetation growth over different stages, which is significant information for vegetation parameter estimation. In addition, these methods are also easily influenced by clouds, aerosols, and water vapor, which could increase the uncertainties of instantaneous remote sensing data and further reduce the accuracy of FVC estimation [21], [41]. To address this issue, in 2016, Wang *et al.* [40] proposed a dynamic Bayesian network (DBN) method using a statistical crop growth model to extract the crop phonological information to estimate FVC from MODIS reflectance data, and indicated the effectiveness of vegetation growth information on improving FVC estimation accuracy. However, this method requires various field survey data to build the crop growth model, which contains the whole time period of vegetation growth.

Currently, time series satellite data containing temporal information provide the potential to use vegetation growth information during FVC estimation processes [42], [43]. In addition, recurrent neural network (RNN), an important branch of deep learning family, has been introduced into the remote sensing community and achieved promising results in hyperspectral image classification, crop yield prediction, and land cover change detection [44]–[46]. Generally, RNN is a powerful neural network that can solve the sequence learning problem using recurrent connections between neural activations over consecutive time steps [44], [47]. According to the sequential time series samples of input and output data, an RNN can effectively sense contextual information and characterize the connection correlation [48]–[50]. Moreover, to solve the vanishing and exploding gradient problems, long short-term memory (LSTM) is proposed to replace the recurrent hidden node memory cell in the RNN [47], [51], [52], which achieved excellent performance on deep sequence learning problems [53], [54]. Therefore, it is reasonable to explore the RNN-LSTM method for FVC estimation, which could effectively extract the vegetation growth information from time series remote sensing data and improve FVC estimation accuracy. According to the characteristic information of vegetation growth, this approach also has potential to weaken the influence of external factors (such as cloud and aerosol contamination) and further improve the robustness of the proposed method.

Therefore, to further improve the spatial resolution of GLASS FVC product, a novel time series FVC estimation algorithm was developed for MODIS 250 m reflectance data using RNN method. In this study, the RNN-LSTM method was adopted to explore the vegetation growth characteristics and incorporate this information into FVC estimation based on the multitemporal MODIS 250 m reflectance and GLASS FVC data. To assess the performance of the proposed method, two popular machine learning methods, including back propagation neural networks (BPNN) and MARS, were also trained and compared with the RNN-LSTM FVC estimation method. Furthermore, the FVC estimations from different methods were also validated using

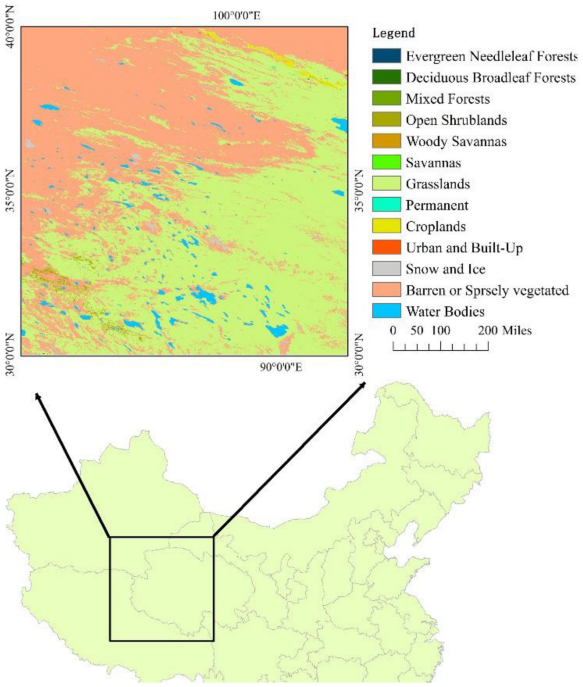

Fig. 1. Geographical location and land cover types of the study area.

high-quality reference FVC data, which were generated by the Advanced Spaceborne Thermal Emission and Reflectance Radiometer (ASTER) data in the Heihe area.

II. Study Area and Data

A. Study Area

The study area is located in mid-west area of China, and it covers approximately 144 million km^2. Fig. 1 shows the geographic location and land cover types of this study area. The terrestrial ecoregions of this area contain montane grasslands and shrublands, Mediterranean forests, woodlands, and scrub [55]. The annual mean temperature and precipitation of this region are 4.1 °C – 8.3 °C and 197 mm, respectively. There are various vegetation types including grass, crops, and woody whose growing seasons are concentrated from May to September in this area.

B. MODIS Data

In this study, MODIS 250 m reflectance data (MOD09Q1, Collection 6) were used as input data for the RNN-LSTM FVC estimation. The MOD09Q1 data are generated from the MODIS-Terra, which is composed of the best observations by Terra during an 8-day interval and considers the overall pixel quality and observational coverage with sinusoidal grid projection [56]. To extract the complete growth characteristics of the vegetation, the whole year reflectance data (2012) of MOD09Q1 were used as time series data for model training. The reflectance data of red (Band 1, 620–670 nm) and NIR (Band 2, 841–876 nm) bands, which had strong sensitivity to vegetation growing state, were selected for FVC estimation [1], [57]. Usually, the seasonal variations and characteristics for different vegetation types are

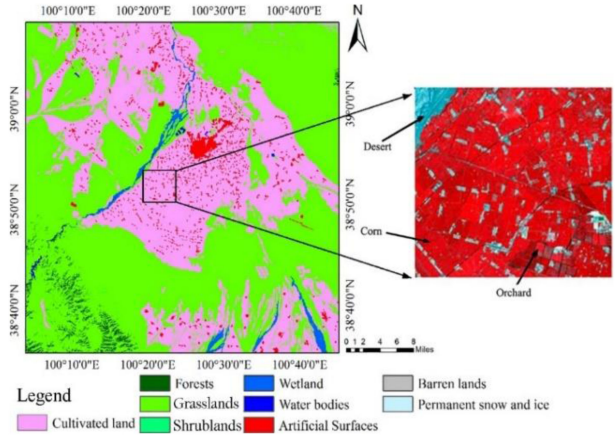

Fig. 2. Geographical location and land cover types of the reference.

different. Thus, the corresponding MODIS land cover data (MCD12Q1, International Geosphere–Biosphere Programme, IGBP) in 2012, were also adopted to discriminate the vegetation types over this study area [58], [59].

C. GLASS FVC Data

The GLASS FVC product is generated from MODIS data (MOD09A1) with the MARS method, which is trained using global distributed high spatial resolution sample data generated from Landsat data [1], [29]. The spatial and temporal resolutions of GLASS FVC product are 500 m and 8 days, respectively. According to global-scale comparison and field validation studies, the GLASS FVC product presents outstanding spatial-temporal continuities and reliable accuracy [28]. Thus, the GLASS FVC data, which were used as the targeted FVC values in training samples, are a suitable choice to develop the RNN-LSTM FVC estimation algorithm. Currently, the GLASS FVC data have been released in the National Earth System Science Data Center.[1]

D. Reference FVC Data in the Heihe Region

To evaluate the accuracy of the proposed algorithm, an independent validation was conducted in the Heihe area, which was located at 38°52′7.5″N and 100°22′10″E and covered approximately 36 km^2 (see Fig. 2) [57], [60]. Generally, the terrain of this region is relatively flat and mainly covered by different kinds of crops. To obtain reliable reference FVC data, Mu *et al.* [61] built an empirical model based on high-spatial-resolution ASTER reflectance data and field FVC measurements. These field FVC measurements were collected from May to September 2012, which covered the whole growing season of these crops in this region. During the ground survey, 22 sampling sites approximately 10 × 10 m in size were selected from this area. Then, nine digital photographs were taken along with two diagonals at each squared sampling site. The FVC value of each photograph was calculated using the Gaussian simulation and segmentation method of the Commission International de L′Eclairage (CIE) Lab color space [62]. Furthermore, the average FVC estimation from these photographs was considered to be the ground FVC

[1]Online. [Available]: http://www.geodata.cn/thematicView/GLASS.html

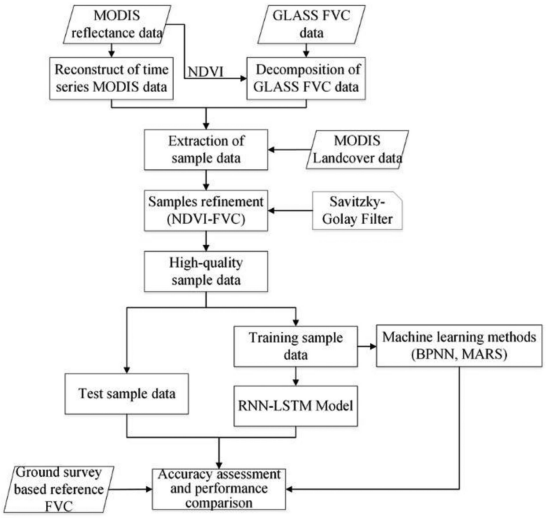

Fig. 3. Flowchart of the RNN-LSTM FVC estimation algorithm.

value of this sampling site. Finally, an empirical transfer function (1) was built based on these ground FVC measurements and the corresponding normalized DVI (NDVI) values derived from the ASTER reflectance data. In this study, the ASTER data of 30th May, 15th June, 10th July, 2nd August, 11th August, and 18th August were used to generate high spatial resolution reference FVC data, which were adopted for the accuracy validation of the proposed algorithm

$$FVC = (a^* NDVI + b)^k \tag{1}$$

where a, b, and k were coefficients of the transfer function which could be determined through the ground FVC measurements and their corresponding NDVI data over these sample sites.

III. Methodology

In this study, the RNN-LSTM method was applied to multitemporal remote sensing data for FVC estimation and Fig. 3 shows the flowchart of this study. First, a cloud detection method was adopted to remove the abnormal values in the MODIS reflectance data, which were affected by the atmosphere and aerosols [63]. Then, a downscaling approach was used to decompose the GLASS FVC data to get the same spatial resolution as MODIS reflectance data [64]. Next, the sequence samples of different vegetation types were extracted according to MODIS land cover data, which were further refined based on the approximately linear relationship between NDVI and FVC data [1]. To ensure the continuity of the FVC estimation, the Savitzky–Golay (SG) filter was used to smooth the refined GLASS FVC data. The samples were randomly divided into two parts. One part, with about 80%, was used to train the RNN-LSTM, BPNN and MARS models, and the remaining one was used to assess the theoretical performances of the trained models. Finally, reference FVC data from Heihe area were adopted to further evaluate the accuracy of the proposed algorithm.

In this study, the RNN-LSTM model was trained using TensorFlow framework, which was implemented on the Linux computer server with Tesla V100 PCIe GPU and 16-GB memory. The BPNN and MARS models were implemented using MATLAB 2015b, which was run on the computer with Intel (R) Core (TM) i7-3770 CPU and 16-GB memory. Particularly, the ARESLab toolbox[2] was adopted to develop the MARS FVC estimation algorithm [65], [66].

A. Data Preprocessing for MODIS Reflectance and GLASS FVC Data

1) Preprocessing of MODIS Reflectance Data: Because of the contamination from residual clouds and shadows, abnormal values might exist in MODIS reflectance data, which would cause spatial-temporal inconsistencies in FVC estimation. In this study, a cloud detection method, time series cloud detection (TSCD), was adopted to the MODIS reflectance data as a preprocessing operation [63]. In this process, the threshold value method was first used to find the clear-sky reference pixels and the remaining pixels were initially labeled as clouds. Because snow usually presented similar reflectance to clouds, confusions of snow and cloud pixels might exist in the initial labeled clouds. Therefore, based on the different reflectance characteristics between snow and cloud on visible and near-infrared (VNIR), and shortwave infrared (SWIR) bands, the MODIS snow mask was refined and used to further discriminate the snow pixels from the initially labeled cloud pixels. Then, these finally labeled cloud contaminated pixels were removed. Next, SG filter method was used based on the clear-sky pixels to fill the removed data. Generally, the SG filter is a polynomial fitting method based on local characteristics of curves and widely used to smooth the time series data [67]. Equation 2 presents the operating principle of SG filter [68]. Finally, continuous and smooth reflectance data were obtained and used to develop the RNN-LSTM FVC estimation algorithm

$$Y_j^* = \frac{\sum_{i=-m}^{i=m} C_i Y_{i+i}}{N} \tag{2}$$

where Y is the original time serious data, Y^* is the smoothed data, C_i is the i*th* correlation coefficient, and the size of smooth window is 2∗m+1.

2) Decomposition of GLASS FVC: Because of the discrepancy of spatial resolution between GLASS FVC and MODIS reflectance data, a downscaling approach was used to decompose the GLASS FVC data in this study [64]. Inspired by the pixel unmixing model, this downscaling approach assumed that each coarse resolution FVC pixel was a linear combination of finer resolution FVC pixels and that all the finer resolution pixels contained in the same coarse resolution pixel were regarded as endmembers of the coarse resolution pixel. The weight of each endmember can be determined by the vegetation growth status. As a popular vegetation index for vegetation growth description, the NDVI was used as the weights of the endmembers in the decomposition process [64]. Fig. 4 shows the diagram of the decomposition approach for GLASS FVC data. First, the NDVI values were derived from the preprocessed MODIS reflectance

[2]Online. [Available]: http://www.cs.rtu.lv/jekabsons/regression.html

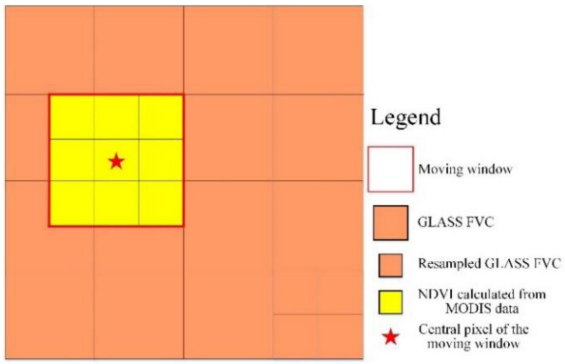

Fig. 4. Flow diagram of the GLASS FVC decomposition approach.

data shown as yellow squares in Fig. 4. In addition, the GLASS FVC was resampled to a 250 × 250 m spatial resolution using bilinear resampling strategy. Then, a moving window with 3 × 3 size, showed as the red box in Fig. 4, started to match the resampled GLASS FVC data pixel by pixel. During this process, the central pixel value of the moving window was calculated using (3), which was treated as the decomposed FVC value. To reduce the interference from nonvegetation, pixels with NDVI values below 0.05 were regarded as nonvegetation and excluded from this decomposition process. Finally, the decomposed FVC data were used to generate the training samples

$$\mathrm{FVC}_C = \frac{\mathrm{NDVI}_C \sum_{i=1}^{M} \mathrm{fvc}_i}{\sum_{i=1}^{M} \mathrm{ndvi}_i} \tag{3}$$

where FVC_C is the decomposed FVC value of the central pixel and NDVI_C is the corresponding NDVI value. M is the number of valid vegetation endmembers within the moving window, and fvc_i and ndvi_i represent the resampled FVC and NDVI values, respectively.

B. Extraction and Refinement of Training Samples

Usually, the seasonal characteristics and statements of different vegetation types vary. Thus, it is essential to build the corresponding FVC estimation models for different vegetation types. In this study, the training samples, which contain the reflectance (red and NIR bands) and targeted FVC values derived from the refined MODIS and decomposed GLASS data, were extracted based on MODIS land cover data. With the statistical information of this study area (see Table I), three main types of vegetation (grass, crops, and open shrublands) were selected to develop the RNN-LSTM FVC estimation method in this study. As for the other types of vegetation, such as evergreen needleleaf forests, deciduous broadleaf forests, mixed forests, etc., as shown in Table I, the model training process was not conducted because of their limited numbers of pixels. During this process, sample pixels of the adopted three vegetation types were selected randomly.

To cover the entire growing season, the sequence reflectance data (red and NIR bands) and GLASS FVC in 2012 for these selected pixels were extracted. Although careful preprocessing was conducted for the MODIS reflectance data and GLASS

TABLE I
STATISTICAL INFORMATION OF THE DIFFERENT VEGETATION TYPES OVER THE STUDY AREA

No	Land types	Present (%)	Count (Pixels)
1	Grasslands	51.35	11831912
2	Open Shrublands	0.54	125028
3	Croplands	0.4	91560
4	Evergreen Needleleaf Forests	3.2×10^{-3}	728
5	Deciduous Broadleaf Forests	5.9×10^{-4}	136
6	Mixed Forests	4.1×10^{-4}	96
7	Woody Savannas	1.1×10^{-3}	256
8	Savannas	4.3×10^{-3}	996
9	Permanent Wetlands	2.1×10^{-2}	4860
10	Nonvegetation	47.68	274610784

FVC product, some abnormal values might still exist, which would exert a negative impact on the FVC estimation accuracy. Thus, a further refinement operation was conducted to refine these training samples. First, the sequence absolute values of the difference data between the FVC and NDVI over these selected pixels were calculated. Based on the approximately linear relationship between the NDVI and FVC, a threshold value of 0.25 was set during this refinement process. The abnormal pixels, which contained values greater than 0.25 over the sequence absolute data, were removed from the training samples. Additionally, an SG filter was adopted to smooth the sequence FVC data. These processes could effectively improve the reliability of the sample data.

C. FVC Estimation Methods

As an extension of traditional neural networks, RNNs have been widely used to address sequence learning problems, and they have achieved good performance in computer vision and remote sensing image interpretations [52], [69], [70]. Generally, an RNN is a feedback forward network with a recurrent unit used to connect the neuron across time, which allows the sharing of parameters across time indexes [52], [71]. In practice, vanishing and exploding gradient problems usually occur in RNNs when they are applied to deep sequence data [72], [73]. To address this problem, LSTM, which modified the structure of the RNN by incorporating self-connected "gates" in the hidden units, was proposed by Hochreiter and Schmidhuber [51]. With these "gates," LSTM is able to collect the relevant information and remove the irrelevant information from deep sequence data [74].

With rigorous preprocessing and refinement for the sequence samples, three RNN-LSTM FVC estimation models for open shrublands, grasslands and croplands were built and utilized to generate regional FVC estimation. The flowchart of the proposed algorithm is shown in Fig. 5. In this study, the number of LSTM cell is 46, and 3 hidden layers are set in each cell, which has 100, 50, and 50 hidden connection nodes, respectively. The optimizer is "adam," training epoch is 500, and learning rate is 0.001. All these optimal values of RNN-LSTM were determined by evaluating the performance of RNN-LSTM model-based R^2 and the root-mean-square error (rmse) indices under different

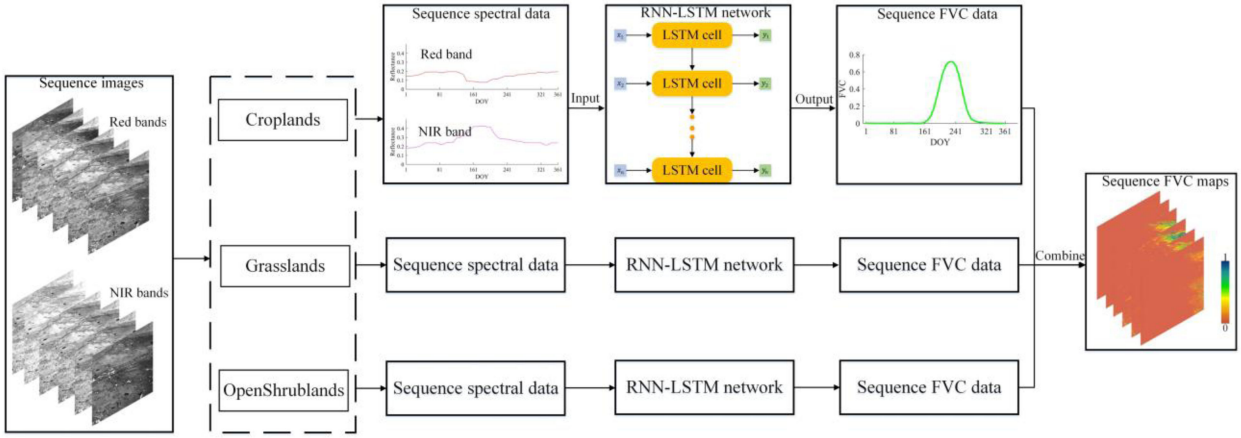

Fig. 5. Flowchart of the RNN-LSTM network for FVC estimation.

values. With these time series remote sensing data, the sequence reflectance data (red and NIR) of each pixel were extracted and fed into the RNN-LSTM network as input data. The output of this algorithm was the sequent FVC estimations, which had the same temporal coverage as the input data.

The BPNN and MARS models were carried out based on MATLAB platform. For BPNN model, the number of hidden layer and nodes could affect the performance of output data. These two parameters were determined by adjusting the values of these two parameters and evaluating the performance of output FVC estimation. After carefully assessment, the optimal number of hidden layer was 2 and the node numbers of each hidden layer are 15 and 8, respectively. The author in [75] provides the detailed information about ARESLab operation for building MARS model. The MARS model was built with the form of the following:

$$f(x) = \sum_{i=1}^{k} c_i B_i(x) \tag{4}$$

$$\begin{cases} \max(0, x - c), x - c > 0 \\ \max(0, c - x), c - x > 0 \end{cases} \tag{5}$$

where $f(x)$ is the corresponding estimation, c_i is a constant coefficient, x is the input vector data, $B_i(x)$ is the piecewise linear basis function. Each piecewise linear basis function was calculated as (5). c is the knot parameter. For MARS model, the key parameters include the knot parameter and number of max basic functions. In this study, we selected the optimal values of these two parameters by valuating the performance of FVC estimation with different parameter values. The final number of basic functions was 21 and the knot content was 3.

IV. Results

A. MODIS Reflectance Data Process

After preprocessing using the TSCD method, the sequence MODIS reflectance data were extracted and evaluated by comparing them with the initial reflectance data. Fig. 6 shows the temporal profiles of the MODIS reflectance data in the red and NIR bands and the NDVI before and after processing over different types of vegetation. Obviously, there were some abnormalities over the initial reflectance data, which showed a sudden variation and would create uncertainties for FVC estimation. Correspondingly, the temporal profiles of the preprocessed data presented smooth variations over time and good consistency with the vegetation growth cycles. Thus, the adopted cloud detection method was capable of addressing the contaminated values in MODIS reflectance data. Moreover, this operation effectively improved the quality of MODIS reflectance data, which is crucial for the accuracy of FVC estimation.

TABLE II
Distribution of the Training Samples in This Study

Types of Vegetation	Total number of samples (pixels)	Number of training samples (pixels)	Number of test samples (pixels)
Open Shrublands	9656	8000	1656
Grasslands	15491	12000	3491
Croplands	14558	12000	2558

B. Training Samples

After careful preprocessing and refinement, high-quality training samples over different types of vegetation were obtained. Fig. 7 shows the density scatter plots between the NDVI and FVC of the training samples over different vegetation types. Generally, the distributions of the FVC values were consistent with the corresponding characteristics of the vegetation types. And the approximately linear relationship between the FVC and NDVI further supported the reliability of the training samples. Moreover, the total number of refined samples and the distribution for training and test processing are shown in Table II. For each vegetation type, over 80% of the sample data were randomly selected for model training, and the remaining data were used to evaluate the theoretical performance of the proposed algorithm.

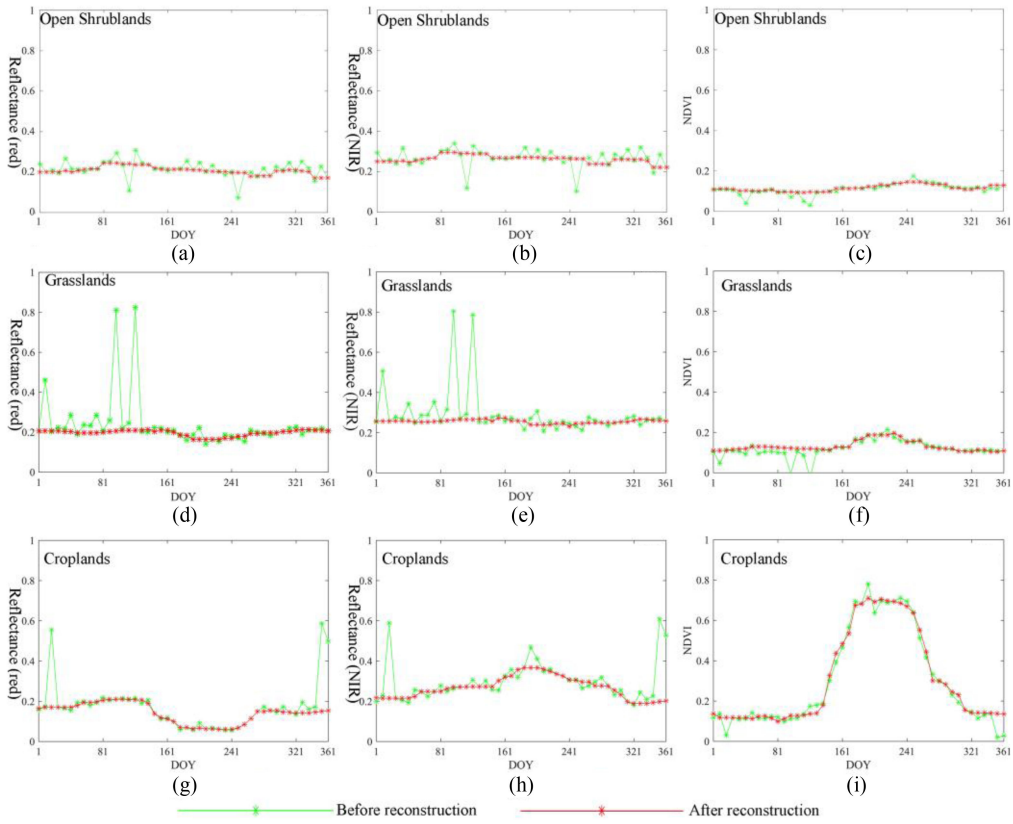

Fig. 6. Temporal profiles of the MODIS reflectance data of the red and NIR bands and the NDVI before and after preprocessing for different types of vegetation.

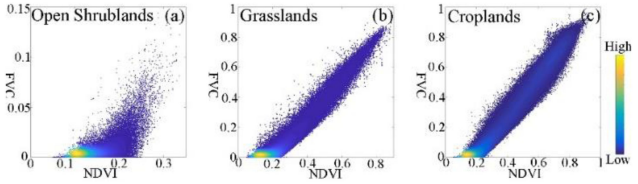

Fig. 7. Density scatter plots of the NDVI from the reconstructed MODIS reflectance data and the refined GLASS FVC of training samples over different vegetation types.

TABLE III
THEORETICAL PERFORMANCES OF THE THREE METHODS

Method	Theoretical performances		
	Open Shrublands	Grasslands	Croplands
BPNN	R^2=0.6248 RMSE=0.0031	R^2=0.9574 RMSE=0.0198	R^2=0.9797 RMSE=0.0347
MARS	R^2=0.383 RMSE=0.0050	R^2=0.9399, RMSE=0.0246	R^2=0.9781 RMSE=0.0370
RNN-LSTM	**R^2=0.7430 RMSE=0.0024**	**R^2=0.9812 RMSE=0.0132**	**R^2=0.9927 RMSE=0.0210**

C. Theoretical Performance Validation

Using the high-quality sample data, different FVC estimation methods were trained over these three types of vegetation. The results of the theoretical performance validation using the test samples are shown in Table III. According to the common assessment indices, including the R-squared (R^2) and rmse, the FVC estimated by the proposed method presented higher accuracy than the BPNN and MARS FVC estimation, which was generated only from the single temporal data. Furthermore, RNN-LSTM FVC estimation also achieved good consistency with the GLASS FVC data. In open shrublands, the proposed algorithm significantly improved the accuracy of the FVC estimation by increasing the R^2 about 0.12 and 0.36 compared with the BPNN and MARS methods, respectively. For grasslands, the accuracy increments of the RNN-LSTM FVC using the rmse and R^2 were approximately 0.007 and 0.03, respectively, compared to the BPNN FVC, and 0.0114 and 0.04, respectively, compared to the MARS FVC. For croplands, the rmse of the RNN-LSTM FVC was reduced by 0.0137 and 0.016 compared with the BPNN and MARS FVC, respectively. According to these satisfactory results, the proposed method has the potential to estimate FVC with reliable accuracy.

D. Spatial-Temporal Comparisons

To assess the spatial performance of the proposed method, the RNN-LSTM FVC estimation of this study area was compared with the corresponding GLASS FVC data. Fig. 8 shows the spatial maps of the RNN-LSTM FVC and GLASS FVC data (DOY = 209). To ensure the spatial completeness of the RNN-LSTM FVC map, the FVC values for nonvegetation pixels, including urban and built-up lands, permanent snow and ice, barren lands, and water bodies, were set to zero. The FVC values for pixels covered by vegetation (evergreen needleleaf forests, deciduous broadleaf forests, mixed forests, open shrublands, hoody savannas, savannas, and permanent wetlands) were filled

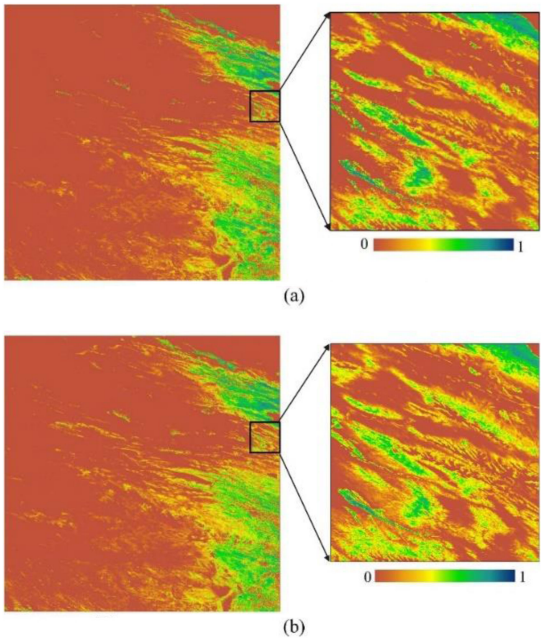

Fig. 8. Spatial distributions and detailed information of the GLASS FVC and RNN-LSTM FVC data over the study area (DOY = 209).

with the decomposed GLASS FVC, respectively. Generally, good spatial agreements between the RNN-LSTM FVC and GLASS FVC were observed in Fig. 8. Furthermore, the spatial distributions of the RNN-LSTM map were consistent with the corresponding vegetation types according to the MODIS land cover data. For example, high FVC values were found over the northeast and southeast regions, which were covered by dense crops and grass. The southwestern area, mainly covered by sporadic open shrublands, grasslands and barren land, showed low FVC values. These results indicated that the proposed method could effectively obtain regional FVC estimation maps with reliable integrity and continuity in both temporal and spatial domains. According to the enlarged map in the local area, the RNN-LSTM FVC map, which benefitted from the improved spatial resolution, presented more detailed spatial variation information about the transitional zones over different land types and better spatial continuity than the GLASS FVC product. Moreover, the spatially smooth transition over different vegetation types of the RNN-LSTM FVC map indicated that the proposed method had enormous potential to conduct large-scale FVC product generation.

To evaluate the temporal performance of the proposed algorithm, the FVC temporal profiles of the RNN-LSTM FVC over different vegetation types were extracted and compared with the corresponding BPNN FVC, MARS FVC, and GLASS FVC products (see Fig. 9). Overall, the varying magnitudes and seasonal variations of the RNN-LSTM FVC data were consistent with the corresponding vegetation types. For example, low FVC values were shown in the RNN-LSTM FVC data for open shrublands over the whole year, except for a slight increase in July and August [see Fig. 9(a) and (b)]. Moreover, clear seasonal changes were observed in the RNN-LSTM FVC for grass and crop vegetation during their growth periods [see Fig. 9(c)–(f)].

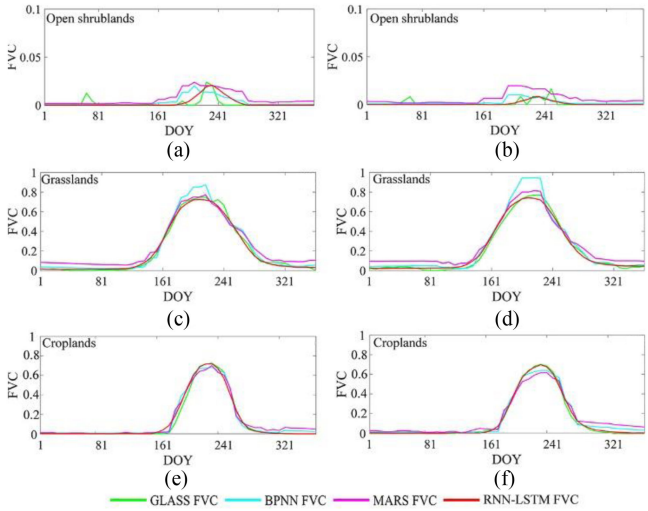

Fig. 9. Temporal profiles of FVC derived by RNN-LSTM, BPNN, and MARS, and GLASS FVC for open shrublands, grasslands, and croplands in this study area.

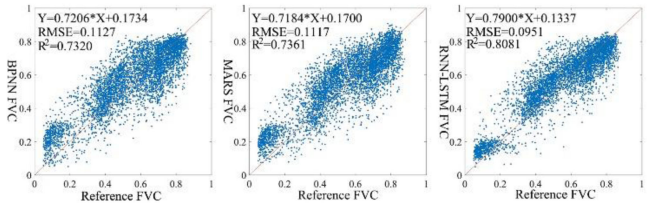

Fig. 10. Scatterplots between the FVC estimations from different methods and the reference data.

These results indicated that the proposed algorithm was effective at describing the temporal characteristics of vegetation growth. Compared with the BPNN and MARS FVC data, these temporal profiles of the RNN-LSTM FVC were closer to the GLASS FVC data, especially at the peak range, which indicated the satisfying temporal consistency between RNN-LSTM FVC and GLASS FVC data. Moreover, the temporal profiles of the RNN-LSTM FVC showed steady variation over time. However, clear fluctuations, which were mainly caused by atmospheric factors and radiation error, were observed in the temporal profiles of the BPNN and MARS FVC data. Based on these results, the proposed algorithm can successfully reduce the effects of external factors and improve the temporal continuity of FVC estimation.

E. Accuracy Validation

To quantitatively evaluate the accuracy of the proposed algorithm, the FVC estimations generated by these three methods were directly compared with the reference FVC data in the Heihe area. Due to the inconsistency of the obtained dates between the FVC estimation and these reference data, the bilinear interpolation method was used to calculate the FVC values on the given dates corresponding to the reference FVC data. The scatterplots of the FVC estimation generated by different methods and the reference FVC values are shown in Fig. 10. Generally, these FVC estimations showed good linear relationships with the reference FVC data, and they approach the 1:1 line. In addition, clear

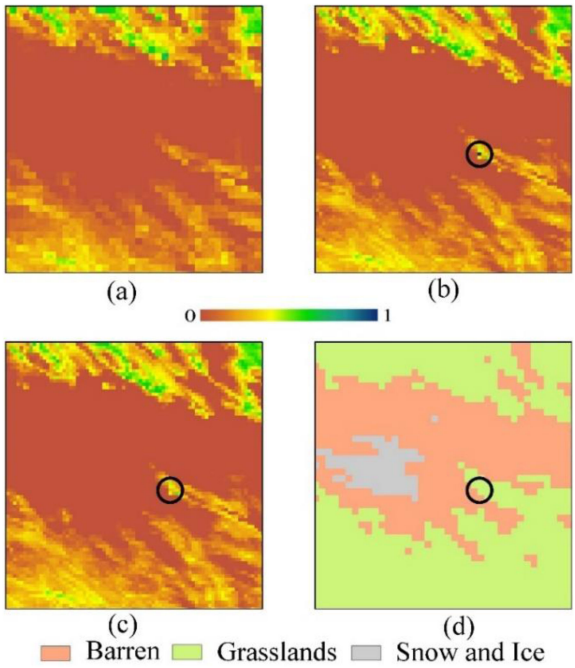

Fig. 11. Partial enlargement map of (a) the GLASS FVC, (b) before processing the RNN-LSTM FVC, (c) after processing the RNN-LSTM FVC, and (d) the MODIS land cover data.

improvements in the FVC estimation accuracy were found in the RNN-LSRM FVC ($R^2 = 0.8081$, rmse $= 0.0951$) compared with the BPNN FVC ($R^2 = 0.7320$, rmse $= 0.1127$) and the MARS FVC ($R^2 = 0.7361$, rmse $= 0.1117$). Moreover, the splattering over low values showed a better concentration, which might benefit from the strong robustness of the RNN-LSTM method for noisy data. These results further indicated that the developed algorithm was capable of generating FVC estimations with reliable accuracy.

V. Discussion

This study proposed a MODIS 250 m FVC estimation algorithm based on the RNN-LSTM method, which could improve the spatial resolution of the GLASS FVC product. This method was capable of extracting the vegetation growth information, which was a significant feature for describing the vegetation state, and incorporate it into time series FVC estimation. Compared to the three common methods of FVC estimation, which only adopted single temporal remote sensing data, this algorithm could effectively reduce the uncertainties caused by clouds, aerosols, and water vapors. In addition, the FVC estimates by the proposed method presented better consistency to the real vegetation state under the natural condition. As a consequence, the proposed method could further improve the temporal consistency and accuracy of FVC estimation. Furthermore, in the partial enlargement maps of the RNN-LSTM FVC (see Figs. 8 and 11), no clear boundary was found over different vegetation types, and the spatial distribution showed excellent continuity, which supported the capacity of the proposed algorithm for large-scale FVC estimation.

In this study, the MCD12Q1 data were adopted as background knowledge to identify the different vegetation types. However, the spatial resolution of MCD12Q1 (500m) does not match the MOD09Q1 data. In practice, the four MOD09Q1 pixels contained by one MCD12Q1 pixel were classified as the same land type of MCD12Q1 in this study. Therefore, there might be some misclassification because of the difference of spatial resolutions between the MCD12Q1 and MOD09Q1 data [76]–[78]. For example, one finer pixel, which was actually covered by barren, might be labeled as grassland at a coarse spatial resolution because it was surrounded by grassy pixels, which would cause considerable errors on FVC estimation. For the spatial-temporal comparisons result, a clearly abnormal pixel was found in the spatial RNN-LSTM FVC estimation map (see the black circle in Fig. 11), which had a particularly higher FVC value than the surrounding pixels. To maintain the spatial continuity, a 5×5 moving window was used to identify and solve these abnormal pixels in this study. In this process, the mean FVC value $\bar{f}$ and variance θ were calculated based on the vegetation pixels in this moving window. In addition, the FVC value of the central pixel, which is out of the $\bar{f} \pm 3\theta$ coverage, is identified as an abnormal value and replaced by $\bar{f}$. Our further work will consider finer land cover data to identify the vegetation types and avoid this error.

In addition, complete annual MODIS reflectance data with 46 images (in 2012) were selected as the time series input data for RNN-LSTM model. Consequently, large amount of computation occurred in model training and FVC generation because of the high dimension of input data. To solve this problem, a highly configured computer server was used to conduct the experiment in this study. Furthermore, there are also potential methods which could be adopted to integrate the temporal information into FVC estimation, such as graph neural network (GNN) [79], [80] and 1-D convolutional neural networks (CNNs) [81]. Therefore, the performance of these methods would be investigated on FVC estimation in the further work.

VI. Conclusion

In this study, a novel FVC estimation algorithm based on the RNN-LSTM method was developed for MODIS 250 m reflectance data. According to the spatial-temporal validation, the proposed method was capable of estimating the FVC with reliable continuity in space and time. In particular, this method could effectively reduce the influence of atmosphere and radiation errors, which was a distinct advantage compared with other FVC estimation methods that only use instantaneous remote sensing data. Furthermore, based on the theoretical performance validation and case study in the Heihe area, improved FVC estimation accuracy was achieved by the proposed method compared with the BPNN and MARS methods.

For future work, there are three potential directions. The first one is expanding the proposed algorithm over large/global scales and conducting extensive assessments for its performance with various vegetation types. The second one is how to extract the spatial information from the sequence remote sensing data and investigate its performance when incorporating it into the FVC

estimation. This study mainly focused on the temporal-spectral information for FVC estimation and neglected the spatial relevance between the neighboring pixels. However, the spatial characteristics are also important information to descript the vegetation growth state. Recently, the CNN, which is an effective means to learn the spatial correlations of remote sensing data, has become a popular method for change detection and land cover classification [82]–[84]. Therefore, the combination of CNN and RNN for sequence FVC estimation would be a promising future direction. Finally, image fusion techniques have been widely used to acquire remote sensing data with high spatial and temporal resolutions [85]–[88], and generating FVC estimation with finer spatial and temporal resolutions based on image fusion techniques is also the further work of this study.

ACKNOWLEDGMENT

The authors would like to thank X. Mu from Beijing Normal University for providing the ground reference FVC data of the Heihe region.

REFERENCES

[1] K. Jia, S. Liang, S. Liu, Y. Li, Z. Xiao, and Y. Yao, "Global land surface fractional vegetation cover estimation using general regression neural networks from MODIS surface reflectance," *IEEE Trans. Geosci. Remote Sens.,* vol. 53, no. 9, pp. 4787–4796, Sep. 2015.

[2] X. Zhang, C. Liao, J. Li, and Q. Sun, "Fractional vegetation cover estimation in arid and semi-arid environments using HJ-1 satellite hyperspectral data," *Int. J. Appl. Earth Observ. Geoinf.,* vol. 21, pp. 506–512, 2013.

[3] K. Jia, B. Wu, Y. Tian, Y. Zeng, and Q. Li, "Vegetation classification method with biochemical composition estimated from remote sensing data," *Int. J. Remote Sens.,* vol. 32, pp. 9307–9325, 2011.

[4] F. Baret, M. Weiss, R. Lacaze, F. Camacho, H. Makhmara, P. Pacholcyzk, "GEOV1: LAI and FAPAR essential climate variables and FCOVER global time series capitalizing over existing products. Part1: Principles of development and production," *Remote Sens. Environ.,* vol. 137, pp. 299–309, 2013.

[5] M. Weiss, F. Baret, R. B. Myneni, A. Pragnère, and Y. Knyazikhin, "Investigation of a model inversion technique to estimate canopy biophysical variables from spectral and directional reflectance data," *Agronomie,* vol. 20, pp. 3–22, 2000.

[6] J. Bian, A. Li, Z. Zhang, W. Zhao, G. Lei, and G. Yin, "Monitoring fractional green vegetation cover dynamics over a seasonally inundated alpine wetland using dense time series HJ-1A/B constellation images and an adaptive endmember selection LSMM model," *Remote Sens. Environ.,* vol. 197, pp. 98–114, 2017.

[7] A. Arneth, "Climate science: Uncertain future for vegetation cover," *Nature,* vol. 524, pp. 44–45, 2015.

[8] M. Barlage and X. Zeng, "The effects of observed fractional vegetation cover on the land surface climatology of the community land model," *J. Hydrometeorol.,* vol. 5, pp. 823–830, 2004.

[9] G. Gutman and A. Ignatov, "The derivation of the green vegetation fraction from NOAA/AVHRR data for use in numerical weather prediction models," *Int. J. Remote Sens.,* vol. 19, pp. 1533–1543, 1998.

[10] X. Zeng, M. Shaikh, Y. Dai, R. E. Dickinson, and R. Myneni, "Coupling of the common land model to the NCAR community climate model," *J. Climate,* vol. 15, pp. 1832–1854, 2002.

[11] R. J. Donohue, M. L. Roderick, and T. R. McVicar, "Can dynamic vegetation information improve the accuracy of Budyko's hydrological model?," *J. Hydrol.,* vol. 390, pp. 23–34, 2010.

[12] M. Jiang, S. Tian, Z. Zheng, Q. Zhan, and Y. He, "Human activity influences on vegetation cover changes in Beijing, China, from 2000 to 2015," *Remote Sens.,* vol. 9, 2017, Art. no. 271.

[13] X. Zeng, R. E. Dickinson, A. Walker, M. Shaikh, R. S. DeFries, and J. Qi, "Derivation and evaluation of global 1-km fractional vegetation cover data for land modeling," *J. Appl. Meteorol.,* vol. 39, pp. 826–839, 2000.

[14] J. Roujean and R. Lacaze, "Global mapping of vegetation parameters from POLDER multiangular measurements for studies of surface-atmosphere interactions: A pragmatic method and its validation," *J. Geophysical Res.*, vol. 107, no. D12, pp. ACL 6-1–ACL 6-14, 2002.

[15] K. Jia, S. Liang, X. Wei, L. Zhang, Y. Yao, and S. Gao, "Automatic land-cover update approach integrating iterative training sample selection and a Markov random field model," *Remote Sens. Lett.,* vol. 5, pp. 148–156, 2014.

[16] J. L. Roujean, M. Leroy, and P. Y. Deschamps, "A bidirectional reflectance model of the earth's surface for the correction of remote sensing data," *J. Geophysical Res. Atmospheres,* vol. 97, pp. 20455–20468, 1992.

[17] F. García-Haro, F. Camacho, A. Verger, and J. Meliá, "Current status and potential applications of the LSA SAF suite of vegetation products," in *Proc. 29th EARSeL Symp.,* Chania, Greece, 2009, pp. 1–8.

[18] J. Jiménez-Muñoz, J. Sobrino, A. Plaza, L. Guanter, J. Moreno, and P. Martínez, "Comparison between fractional vegetation cover retrievals from vegetation indices and spectral mixture analysis: Case study of PROBA/CHRIS data over an agricultural area," *Sensors,* vol. 9, pp. 768–793, 2009.

[19] C. Bacour, F. Baret, D. Béal, M. Weiss, and K. Pavageau, "Neural network estimation of LAI, fAPAR, fCover and LAI × Cab, from top of canopy MERIS reflectance data: Principles and validation," *Remote Sens. Environ.,* vol. 105, pp. 313–325, 2006.

[20] F. Baret, O. Hagolle, B. Geiger, P. Bicheron, B. Miras, M. Huc, "LAI, fAPAR and fCover CYCLOPES global products derived from VEGETATION: Part 1: Principles of the algorithm," *Remote Sens. Environ.,* vol. 110, pp. 275–286, 2007.

[21] F. Baret, K. Pavageau, D. Béal, M. Weiss, B. Berthelot, and P. Regner, "Algorithm theoretical basis document for MERIS top of atmosphere land products (TOA_VEG)," INRA-CSE*:* Avignon, France*,* 2006.

[22] F. García-Haro, S. Sommer, and T. Kemper, "A new tool for variable multiple endmember spectral mixture analysis (VMESMA)," *Inter. J. Remote Sensing*, vol. 26, no. 10, pp. 2135–2162, 2005.

[23] J. B. Adams, M. O. Smith, and P. E. Johnson, "Spectral mixture modeling: A new analysis of rock and soil types at the Viking Lander 1 site," *J. Geophysical Res., Solid Earth,* vol. 91, pp. 8098–8112, 1986.

[24] A. Verger, "Comparison and analysis of operational algorithms estimating biophysical parameters of the vegetation cover," *Dept. Phys. Earth Thermodynam.*, p. 277. Valencia, Spain: University of Valencia.

[25] A. Verger, F. Baret, and M. Weiss, "GEOV2/VGT: Near real time estimation of global biophysical variables from VEGETATION-P data," in *Proc. 7th Int. Workshop Anal. Multi-temporal Remote Sens. Images*, 2013, pp. 1–4.

[26] F. Camacho, J. Sánchez, R. Lacaze, M. Weiss, F. Baret, and A. Verger, "Validating GEOV3 LAI, FAPAR and vegetation cover estimates derived from PROBA-V observations at 333m over Europe," in *Proc. EGU General Assem. Conf. Abstr.*, pp. EPSC2016–14917, 2016.

[27] F. Camacho, J. Cernicharo, R. Lacaze, F. Baret, and M. Weiss, "GEOV1: LAI, FAPAR essential climate variables and FCOVER global time series capitalizing over existing products. Part 2: Validation and intercomparison with reference products," *Remote Sens. Environ.,* vol. 137, pp. 310–329, 2013.

[28] D. Liu, K. Jia, X. Wei, M. Xia, X. Zhang, and Y. Yao, "Spatiotemporal comparison and validation of three global-scale fractional vegetation cover products," *Remote Sens.,* vol. 11, 2019, Art. no. 2524.

[29] L. Yang, K. Jia, S. Liang, J. Liu, and X. Wang, "Comparison of four machine learning methods for generating the GLASS fractional vegetation cover product from MODIS data," *Remote Sens.,* vol. 8, 2016, Art. no. 682.

[30] J. L. Roujean and R. Lacaze, "Global mapping of vegetation parameters from POLDER multiangular measurements for studies of surface-atmosphere interactions: A pragmatic method and its validation," *J. Geophysical Res., Atmos.,* vol. 107, pp. ACL 6–1–ACL 6–14, 2002.

[31] L. Gao, X. Wang, B. A. Johnson, Q. Tian, Y. Wang, and J. Verrelst, "Remote sensing algorithms for estimation of fractional vegetation cover using pure vegetation index values: A review," *ISPRS J. Photogrammetry Remote Sens.,* vol. 159, pp. 364–377, 2020.

[32] G. Jiapaer, X. Chen, and A. Bao, "A comparison of methods for estimating fractional vegetation cover in arid regions," *Agricultural Forest Meteorol.,* vol. 151, pp. 1698–1710, 2011.

[33] X. Mu, W. Song, Z. Gao, T. R. McVicar, R. J. Donohue, and G. Yan, "Fractional vegetation cover estimation by using multi-angle vegetation index," *Remote Sens. Environ.,* vol. 216, pp. 44–56, 2018.

[34] D. Lyu, B. Liu, X. Zhang, X. Yang, L. He, and J. He, "An experimental study on field spectral measurements to determine appropriate daily time for distinguishing fractional vegetation cover," *Remote Sens.,* vol. 12, 2020, Art. no. 2924.

[35] I. D. Dobreva and A. G. Klein, "Fractional snow cover mapping through artificial neural network analysis of MODIS surface reflectance," *Remote Sens. Environ.,* vol. 115, pp. 3355–3366, 2011.

[36] E. H. Czyzowska-Wisniewski, W. J. van Leeuwen, K. K. Hirschboeck, S. E. Marsh, and W. T. Wisniewski, "Fractional snow cover estimation in complex alpine-forested environments using an artificial neural network," *Remote Sens. Environ.,* vol. 156, pp. 403–417, 2015.

[37] S. Kuter, Z. Akyurek, and G.-W. Weber, "Retrieval of fractional snow covered area from MODIS data by multivariate adaptive regression splines," *Remote Sens. Environ.,* vol. 205, pp. 236–252, 2018.

[38] S. Kuter, "Completing the machine learning saga in fractional snow cover estimation from MODIS terra reflectance data: Random forests versus support vector regression," *Remote Sens. Environ.,* vol. 255, 2021, Art. no. 112294.

[39] Y. Tu, K. Jia, X. Wei, Y. Yao, M. Xia, and X. Zhang, "A time-efficient fractional vegetation cover estimation method using the dynamic vegetation growth information from time series GLASS FVC product," *IEEE Geosci. Remote Sens. Lett.,* vol. 17, no. 10, pp. 1672–1676, Oct. 2020.

[40] X. Wang, K. Jia, S. Liang, and Y. Zhang, "Fractional vegetation cover estimation method through dynamic Bayesian network combining radiative transfer model and crop growth model," *IEEE Trans. Geosci. Remote Sens.,* vol. 54, no. 12, pp. 7442–7450, Dec. 2016.

[41] J. Xiao and A. Moody, "A comparison of methods for estimating fractional green vegetation cover within a desert-to-upland transition zone in central new Mexico, USA," *Remote Sens. Environ.,* vol. 98, pp. 237–250, 2005.

[42] F. Grings, E. Roitberg, and V. Barraza, "EVI time-series breakpoint detection using convolutional networks for online deforestation monitoring in Chaco forest," *IEEE Trans. Geosci. Remote Sens.,* vol. 58, no. 2, pp. 1303–1312, Feb. 2020.

[43] X. Zhan, Z. Xiao, J. Jiang, and H. Shi, "A data assimilation method for simultaneously estimating the multiscale leaf area index from time-series multi-resolution satellite observations," *IEEE Trans. Geosci. Remote Sens.,* vol. 57, no. 11, pp. 9344–9361, Nov. 2019.

[44] L. Mou, P. Ghamisi, and X. X. Zhu, "Deep recurrent neural networks for hyperspectral image classification," *IEEE Trans. Geosci. Remote Sens.,* vol. 55, no. 7, pp. 3639–3655, Jul. 2017.

[45] A. W. Sugiyarto and A. M. Abadi, "Prediction of Indonesian palm oil production using long short-term memory recurrent neural network (LSTM-RNN)," in *Proc. 1st Int. Conf. Artif. Intell. Data Sci.*, 2019, pp. 53–57.

[46] L. Mou and X. X. Zhu, "A recurrent convolutional neural network for land cover change detection in multispectral images," in *Proc. IEEE Int. Geosci. Remote Sens. Symp.*, 2018, pp. 4363–4366.

[47] F. Zhou, R. Hang, Q. Liu, and X. Yuan, "Hyperspectral image classification using spectral-spatial LSTMs," *Neuro Computing*, vol. 328, pp. 39–47, 2019.

[48] X. Fu, S. Li, M. Fairbank, D. C. Wunsch, and E. Alonso, "Training recurrent neural networks with the Levenberg–Marquardt algorithm for optimal control of a grid-connected converter," *IEEE Trans. Neural Netw. Learn. Syst.,* vol. 26, no. 9, pp. 1900–1912, Sep. 2015.

[49] A. Ma, A. M. Filippi, Z. Wang, Z. Yin, D. Huo, and X. Li, "Fast sequential feature extraction for recurrent neural network-based hyperspectral image classification," *IEEE Trans. Geosci. Remote Sens.,* to be published.

[50] H. Chen, C. Wu, B. Du, L. Zhang, and L. Wang, "Change detection in multisource VHR images via deep siamese convolutional multiple-layers recurrent neural network," *IEEE Trans. Geosci. Remote Sens.,* vol. 58, no. 4, pp. 2848–2864, Apr. 2020.

[51] S. Hochreiter and J. Schmidhuber, "Long short-term memory," *Neural Comput.,* vol. 9, pp. 1735–1780, 1997.

[52] R. Williams and D. Zipser, "A learning algorithm for continually running fully recurrent neural networks," *Neural Comput.,* vol. 1, pp. 270–280, 2014.

[53] F. Zhou, R. Hang, Q. Liu, and X. Yuan, "Hyperspectral image classification using spectral-spatial LSTMs," *Neurocomputing,* vol. 328, pp. 39–47, 2019.

[54] S. Srivastava and S. Lessmann, "A comparative study of LSTM neural networks in forecasting day-ahead global horizontal irradiance with satellite data," *Sol. Energy,* vol. 162, pp. 232–247, 2018.

[55] D. M. Olson, E. Dinerstein, E. D. Wikramanayake, N. D. Burgess, G. V. N. Powell, and E. C. Underwood, "Terrestrial ecoregions of the world: A new map of life on earth: A new global map of terrestrial ecoregions provides an innovative tool for conserving biodiversity," *BioScience,* vol. 51, pp. 933–938, 2001.

[56] L. NASA, "DAAC: ASTER level 1 precision terrain corrected registered at-sensor radiance, version 3, NASA EOSDIS land processes DAAC," USGS Earth Resour. Obser. Sci. Center, Sioux Falls, South Dakota.

[57] D. Liu, L. Yang, K. Jia, S. Liang, Z. Xiao, and X. Wei, "Global fractional vegetation cover estimation algorithm for VIIRS reflectance data based on machine learning methods," *Remote Sens.,* vol. 10, 2018, Art. no. 1648.

[58] M. A. Friedl, D. Sulla-Menashe, B. Tan, A. Schneider, N. Ramankutty, and A. Sibley, "MODIS collection 5 global land cover: Algorithm refinements and characterization of new datasets," *Remote Sens. Environ.,* vol. 114, pp. 168–182, 2010.

[59] D. Sulla-Menashe and M. A. Friedl, "User guide to collection 6 MODIS land cover (MCD12Q1 and MCD12C1) product," USGS: Reston, VA, USA, 2018, pp. 1–18.

[60] J. Chen, A. Liao, J. Chen, S. Peng, L. Chen, and H. Zhang, "30-meter global land cover data product-GlobeLand30," *Geomatics World,* vol. 24, pp. 1–8, 2017.

[61] X. Mu, S. Huang, H. Ren, G. Yan, W. Song, and G. Ruan, "Validating GEOV1 fractional vegetation cover derived from coarse-resolution remote sensing images over croplands," *IEEE J. Sel. Topics Appl. Earth Observ. Remote Sens.,* vol. 8, no. 4, pp. 439–446, Apr. 2014.

[62] Y. Liu, X. Mu, H. Wang, and G. Yan, "A novel method for extracting green fractional vegetation cover from digital images," *J. Vegetation Sci.,* vol. 23, pp. 406–418, 2012.

[63] H. Tang, K. Yu, O. Hagolle, K. Jiang, X. Geng, and Y. Zhao, "A cloud detection method based on a time series of MODIS surface reflectance images," *Int. J. Digit. Earth,* vol. 6, pp. 157–171, 2013.

[64] Y. Tu, K. Jia, S. Liang, X. Wei, Y. Yao, and X. Zhang, "Fractional vegetation cover estimation in heterogeneous areas by combining a radiative transfer model and a dynamic vegetation model," *Int. J. Digit. Earth,* vol. 13, no. 4, pp. 487–503, 2020.

[65] G. Jekabsons, "ARESLab: Adaptive regression splines toolbox for Matlab/Octave," 2011. [Online]. Available: http://www. cs. rtu. lv/jekabsons

[66] G. Jekabsons, "ARESLab: Adaptive regression splines toolbox for Matlab/Octave (ver. 1.10. 3)," Latvia: Institute of Applied Computer Systems Riga Technical Univ. 2016. [Online]. Available: from: http://www. cs. rtu. lv/jekabsons/Files/ARESLab. pdf

[67] R. W. Schafer, "What is a Savitzky-Golay filter," *IEEE Signal Process. Mag.,* vol. 28, no. 4, pp. 111–117, Jul. 2011.

[68] J. Chen, P. Jönsson, M. Tamura, Z. Gu, B. Matsushita, and L. Eklundh, "A simple method for reconstructing a high-quality NDVI time-series data set based on the Savitzky–Golay filter," *Remote Sens. Environ.,* vol. 91, pp. 332–344, 2004.

[69] P. Rodriguez, J. Wiles, and J. L. Elman, "A recurrent neural network that learns to count," *Connection Sci.,* vol. 11, pp. 5–40, 1999.

[70] Y. LeCun, Y. Bengio, and G. Hinton, "Deep learning," *Nature,* vol. 521, pp. 436–444, 2015.

[71] X. X. Zhu, D. Tuia, L. Mou, G. S. Xia, L. Zhang, and F. Xu, "Deep learning in remote sensing: A review," vol. 5, no. 4, pp. 8–36, Dec. 2017.

[72] S. Srivastava and S. Lessmann, "A comparative study of LSTM neural networks in forecasting day-ahead global horizontal irradiance with satellite data," *Sol. Energy,* vol. 162, pp. 232–247, 2018.

[73] Y. Bengio, "Learning long-term dependencies with gradient descent is difficult," *IEEE Trans. Neural Netw.,* vol. 5, no. 2, pp. 157–166, Mar. 1994.

[74] S. Hochreiter, Y. Bengio, P. Frasconi, and J. Schmidhuber, "Gradient flow in recurrent nets: The difficulty of learning long-term dependencies," in *a Field Guide to Dynamical Recurrent Neural Networks*. Piscataway, NJ, USA:IEEE Press, 2001.

[75] J. H. Friedman, "Multivariate adaptive regression splines," in *The Annals of Statistics*, vol. 19, no. 1, 1991, pp. 1–67. JSTOR, www.jstor.org/stable/2241837. Accessed 10 May 2021.

[76] H. Wu and Z.-L. Li, "Scale issues in remote sensing: A review on analysis, processing and modeling," *Sensors,* vol. 9, pp. 1768–1793, 2009.

[77] Y. Bo and J. Wang, "Exploring the scale effect in thematic classification of remotely sensed data: The statistical separability-based method," *Remote Sens. Technol. Appl.,* vol. 19, pp. 443–449, 2011.

[78] C. Fern and T. A. Warner, "Scale and texture in digital image classification," *Photogrammetric Eng. Remote Sens.,* vol. 68, pp. 51–63, 2002.

[79] Y. Li, R. Chen, Y. Zhang, M. Zhang, and L. Chen, "Multi-Label remote sensing image scene classification by combining a convolutional neural network and a graph neural network," *Remote Sens.,* vol. 12, 2020, Art. no. 4003.

[80] Y. Zhang, X. Dong, L. Shang, D. Zhang, and D. Wang, "A multi-modal graph neural network approach to traffic risk forecasting in smart urban sensing," in *Proc. 17th Annu. IEEE Int. Conf. Sens., Commun., Netw.*, 2020, pp. 1–9.

[81] J. Yan, J. Meng, and J. Zhao, "Real-time bottom tracking using side scan sonar data through one-dimensional convolutional neural networks," *Remote Sens.,* vol. 12, 2020, Art. no. 37.

[82] C. Kwan, B. Ayhan, B. Budavari, Y. Lu, D. Perez, and J. Li, "Deep learning for land cover classification using only a few bands," *Remote Sens.,* vol. 12, pp. 2020, Art. no. 2000.
[83] C. Kwan, D. Gribben, B. Ayhan, S. Bernabe, A. Plaza, and M. Selva, "Improving land cover classification using extended multi-attribute profiles (EMAP) enhanced color, near infrared, and LiDAR data," *Remote Sens.,* vol. 12, 2020, Art. no. 1392.
[84] B. Ayhan, C. Kwan, J. Larkin, L. Kwan, D. Skarlatos, and M. Vlachos, "Deep learning model for accurate vegetation classification using RGB image only," *Proc. SPIE*, vol. 11398, 2020, Art. no. 113980H.
[85] C. Kwan, B. Budavari, F. Gao, and X. Zhu, "A hybrid color mapping approach to fusing MODIS and Landsat images for forward prediction," *Remote Sens.,* vol. 10, 2018, Art. no. 520.
[86] C. Kwan, X. Zhu, F. Gao, B. Chou, D. Perez, and J. Li "Assessment of spatiotemporal fusion algorithms for planet and worldview images," *Sensors,* vol. 18, 2018, Art. no. 1051.
[87] J. Xue, Y. Leung, and T. Fung, "An unmixing-based bayesian model for spatio-temporal satellite image fusion in heterogeneous landscapes," *Remote Sens.,* vol. 11, 2019, Art. no. 324.
[88] J. Ma, W. Zhang, A. Marinoni, L. Gao, and B. Zhang, "An improved spatial and temporal reflectance unmixing model to synthesize time series of landsat-like images," *Remote Sens.,* vol. 10, 2018, Art. no. 1388.

Duanyang Liu received the B.S. degree in remote sensing science and technology from Southwest Jiaotong University, Chengdu, China, in 2017, the M.S. degree in cartography and geography information system from Beijing Normal University, Beijing, China, in 2021.

He is currently with the State Key Laboratory of Remote Sensing Science and the Beijing Engineering Research Center for Global Land Remote Sensing Products, Faculty of Geographical Science, Beijing Normal University. His main research interests include fractional vegetation cover retrieval and remote sensing data processing and analysis.

Kun Jia received the B.S. degree in surveying and mapping engineering from Central South University, Changsha, China in 2006, the Ph.D. degree in cartography and GIS from the Institute of Remote Sensing Applications, Chinese Academy of Sciences, Beijing, China, in 2011.

He is currently an Associate Professor with the State Key Laboratory of Remote Sensing Science and also the Beijing Engineering Research Center for Global Land Remote Sensing Products, Faculty of Geographical Science, Beijing Normal University, Beijing, China. His main research interests include estimation of vegetation parameters, land cover classification, and agriculture monitoring using remote sensing data.

Mu Xia received the B.S. degree in geographic information system from China University of Geosciences, Beijing, China, in 2013, the M.A. degree in environmental remote sensing and geographic information system from Boston University, Boston, MA, USA, in 2015. She is currently pursuing the Ph.D. degree in cartography and geography information system with the State Key Laboratory of Remote Sensing Science and the Beijing Engineering Research Center for Global Land Remote Sensing Products, Faculty of Geographical Science, Beijing Normal University, Beijing, China.

Her main research interests include environmental remote sensing and ecological evaluation using remote sensing data.

Xiangqin Wei received the Ph.D. degree in cartography and geography information system from the Institute of Remote Sensing and Digital Earth, Chinese Academy of Sciences, Beijing, China, in 2017.

She is currently an Associate Professor with Aerospace Information Research Institute, Chinese Academy of Sciences, Beijing, China, and the Remote Sensing Satellite Applications, National Engineering Laboratory, China. Her research interests include ecological monitoring with remote sensing and application of quantitative remote sensing.

Yunjun Yao received the Ph.D. degree in cartography and geography information system from Peking University, Beijing, China, in 2010. From October 2008 until October 2009, he was with the Department of Geographical Sciences, University of Maryland, College Park, MD, USA, as a joint Ph.D. student.

He is currently with the State Key Laboratory of Remote Sensing Science, Faculty of Geographical Science, Beijing Normal University, Beijing, China. His main research interests include estimation of evapotranspiration and retrieval of surface biophysical parameters by remote sensing.

Xiaotong Zhang received the Ph.D. degree in cartography and geographical information science from Wuhan University, Wuhan, China, in 2010.

He was with the Department of Geographical Sciences, University of Maryland, College Park, MD, USA, as a Joint Ph.D. Student. He is currently with the State Key Laboratory of Remote Sensing Science, Faculty of Geographical Science, Beijing Normal University, Beijing, China. His main research interests include estimation of land surface radiation components from satellite data, as well as Earth energy balance.

Guofeng Tao received the B.S. degree in geographic information science from Central China Normal University, Wuhan, China, in 2019. She is currently working toward the Ph.D. degree in cartography and geography information system in the State Key Laboratory of Remote Sensing Science, Faculty of Geographical Science, Beijing Normal University, Beijing, China.

Her main research interests include fractional vegetation cover retrieval and spatiotemporal fusion.